Coordinated Secondary Control for Balanced Discharge Rate of Energy Storage System in Islanded AC Microgrids

Guan, Yajuan; Quintero, Juan Carlos Vasquez; Guerrero, Josep M.

Published in:
I E E E Transactions on Industry Applications

DOI (link to publication from Publisher):
10.1109/TIA.2016.2598724

Publication date:
2016

Document Version
Early version, also known as pre-print

Coordinated Secondary Control for Balanced Discharge Rate of Energy Storage System in Islanded AC Microgrids

Yajuan Guan
Student Member, IEEE
Aalborg University
Pontoppidanstraede 111
Aalborg, 9220, Denmark
ygu@et.aau.dk

Juan C. Vasquez
Senior Member, IEEE
Aalborg University
Pontoppidanstraede 111
Aalborg, 9220, Denmark
juq@et.aau.dk

Josep M. Guerrero
Fellow, IEEE
Aalborg University
Pontoppidanstraede 111
Aalborg, 9220, Denmark
joz@et.aau.dk

***Abstract* -- A coordinated secondary control approach based on an autonomous current-sharing control strategy for balancing the discharge rates of energy storage systems (ESSs) in islanded AC microgrids is proposed in this paper. The coordinated secondary controller can regulate the power outputs of distributed generation (DG) units according to their states-of-charge (SoCs) and ESS capacities by adjusting the virtual resistances of the paralleled voltage-controlled inverters. Compared with existing controllers, the proposed control strategy not only effectively prevents operation failure caused by overcurrent incidents and unintentional outages in DG units, but also aims to provide a fast transient response and an accurate output-current-sharing performance. A complete root locus analysis is given in order to achieve system stability and parameter sensitivity. Experimental results are presented to show the performance of the whole system and to verify the effectiveness of the proposed controller.**

***Index Terms*— Coordinated secondary control, energy storage system, balanced discharge rate, autonomous current-sharing control, microgrids**

I. INTRODUCTION

Nowadays, environmental issues, uncertainty in prices of fossil fuels, concerns about power supply security, and liberalization of electricity markets, have resulted in significant changes in power systems. Compared to traditional central power plants, small-scale distributed generation (DG) systems are receiving more considerable interest because of several renewable energy use case scenarios and applications [1]-[3].

Microgrids (MGs) have been proposed as an emerging for generating electricity thanks to their renewable energy sources (RESs) on-site integration [4]-[13]. According to the definition of the Consortium for Electric Reliability Technology Solutions (CERTS), MGs should be able to supply local sensitive loads without the support of a main grid [14]. Therefore, energy storage systems (ESSs) play an important role for MGs as they should be charged either by a utility grid or by RESs. Furthermore, the ESSs should be able to overcome the intermittent nature of RESs and also, to support local loads during grid failure and electrical shortage. ESSs should be used and therefore, discharged for peak shaving purposes, enhancing both system stability and reliability [15]-[17]. However, a trade-off is depicted between cost and system reliability because an ESS is usually one of the most expensive components in an MG [18]. Optimal sizing methodologies for ESSs have been proposed to avoid over-charge and deep-discharge which may lead to permanent damages [19], [20]. Finally, a control strategy for balancing the discharge rates is necessary, especially when the ESS capacities in an MG are different.

The ESS controllability is limited by the energy capacity of its storage device. If the ESSs are the only mechanisms involved in controlling the stability and reliability of the MG, then an operation failure may occur. This setback may occur because the available electrical energy from ESSs is affected by various factors, such as charging and discharging conditions, ambient temperature, current charge and discharge cycles, and aging [21]-[25]. The conventional power-sharing control strategies mainly focus on the equalization of power-sharing among DG units [8]-[13]. However, the ESSs in different DG units could have different discharge rates according to their states-of-charge (SoCs) and capacities. A powerless DG unit can be shut down first when its SoC is below the threshold, and the remaining DG units have to supply more power to the total loads. This situation would probably cause overcurrent and unintentional outages. Furthermore, it could degrade the stability and reliability of the MG. All aspects of the coordinated power output control strategy, such as the SoC and ESS capacities, should be considered. The unit with the highest SoC should supply more power to the common load to ensure a balanced discharge rate. This coordinated control strategy can be integrated into a hierarchical structure with a central controller and a local controller [26]-[29]. The primary control can regulate the output voltage of each DG unit based on the commands sent from a high-level controller. Several coordinated control strategies for SoC balancing in an MG have been established by combining communication technology and hierarchical control [30]-[36]. A coordinated SoC control for distributed ESSs by using adaptive droop control in DC MGs has been proposed in [30]. In [31], an adaptive virtual resistance (VR) based droop controller was proposed to achieve stored-energy balancing. Further, a voltage scheduling droop method was proposed to maintain the SoC balance for the ESSs in [32]. Another research direction was taken by using fuzzy logic-based control

strategy as presented in [33]-[35] for a DC MG by modifying the droop gains. Alternatively, a distributed multi-agent-based algorithm was proposed in [36] to achieve SoC balancing by using voltage scheduling.

However, the aforementioned control strategies were all developed for implementation in DC MGs. Furthermore, most of these methods rely on droop control, which has a relatively slow transient response in AC MGs caused by the averaged active and reactive power calculation when using low-pass filters as shown in [37]. In addition, both adaptive droop coefficients and variable voltage references seriously affect system stability in droop-controlled systems [38], [39].

In view of these issues, a novel coordinated secondary control strategy for balancing the discharge rates of ESSs in islanded AC MGs is proposed in this paper. The coordinated controller can prevent overcurrent incidents and unintentional outages in DG units by regulating the power outputs of the DG units according to their SoCs. The control strategy aims to adjust the VRs of the voltage controlled inverters (VCIs) at the secondary level in terms of SoC and ESS capacities. An autonomous current-sharing controller is integrated in primary control to ensure a fast and accurate load sharing performance of paralleled VCIs. The proposed coordinated secondary controller can provide a larger stability margin than the conventional droop controller. Root locus analysis is presented to analyze stability and parameter sensitivity.

The rest of the paper is organized as follows: Section II introduces the islanded AC MG configuration and ESS characteristics. Section III presents the proposed discharge rate balancing control and the primary control strategy. Section IV illustrates the linearized state-space model and stability analysis. Section V presents the simulation and experimental results. Section VI concludes the paper.

II. Islanded AC MG and ESS Characteristics

A. *Islanded MG Configuration*

A photovoltaic (PV)-ESS-based islanded AC MG case-study scenario is shown in Fig. 1. The MG consists of DG units, local loads, ESSs, and control loops. Each DG unit includes a DC/DC converter and a three-phase VCI connected to the AC bus. The DG units are powered by PV panels and ESSs. The coordinated secondary control for SoC balancing requires an MG central controller (MGCC) which consists of slow control loops and low-bandwidth communication links, to collect measurements and relay the control signals to each DG unit.

In daylight, the ESS can operate in either charging or discharging mode according to the power outputs of PV panels and consumption. The main function of the ESS during the day is to balance the power between the RESs and local loads. At night, the ESS is a grid-forming unit because of the lack of solar energy. In this scenario, only ESSs are needed to provide the stability and reliability of the islanded MG. The power outputs of the DG units should be coordinated in order to share the load in accordance with their SoC and ESS capacities and consequently to prevent operation failure of MGs.

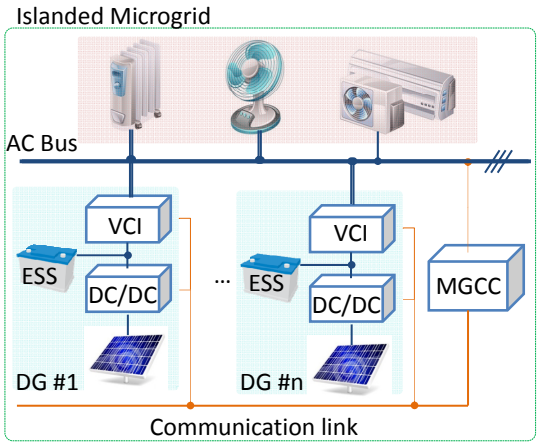

Fig. 1. A PV-ESS based MG case-study scenario.

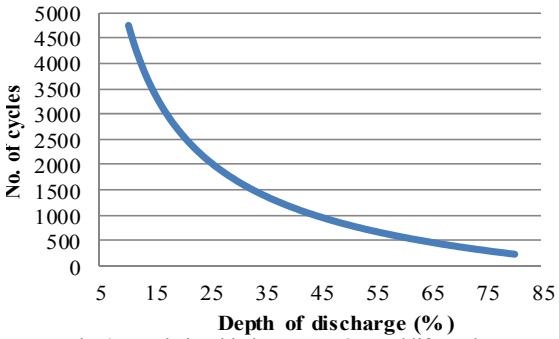

Fig. 2. Relationship between DOD and life cycles.

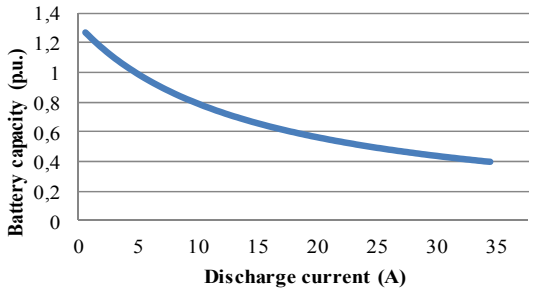

Fig. 3. Relationship between the discharge current and nominal capacity.

B. *ESS Characteristics*

In this paper, valve-regulated lead acid (VRLA) batteries are considered as a power source for the ESSs because VRLA battery allows for a considerable number of charge-discharge cycles, deep-discharge capability and low cost.

However, one of the most important issues on VRLA batteries is the contradiction between the depth of discharge (DOD) and cycle life, as shown in Fig. 2. The number of cycles yielded by a VRLA battery increases exponentially the shallow DOD. Therefore, there is a limitation for SoC to prevent of deep-discharge in practice. However, according to the nonlinear and immeasurable nature of SoC, some

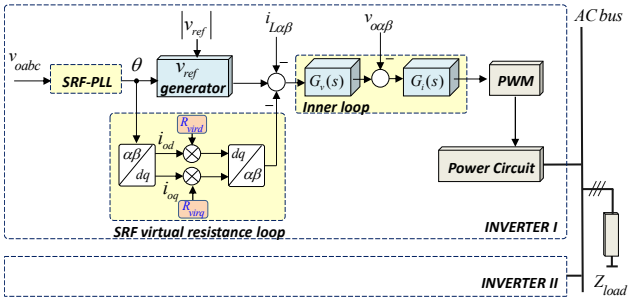

Fig. 4. The autonomous current-sharing control strategy.

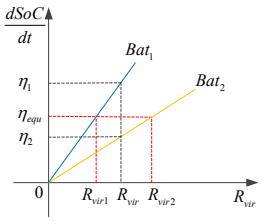

Fig. 5. Control principle for discharge rates balancing.

complex models and advanced algorithms have been proposed to increase the accuracy of SoC prediction.

Another issue with VRLA batteries is the relationship between nominal capacity and discharge current, as depicted in Fig. 3. The capacity in the battery declines exponentially with an increase of discharge current. This phenomenon shows that the total available electrical energy in a VRLA battery may vary according to the discharge condition even if the batteries have the same initial SoC. Therefore, the ESS with a smaller discharge current and balanced discharge rate may work for a longer time than an ESS with the equal power-sharing control.

III. Proposed Discharge Rate Balancing Control

A. Primary Control for Current- and Power-sharing

The autonomous current-sharing control strategy used at the primary level is depicted in Fig. 4 [40]. The controller includes a VR loop (R_{vird} and R_{virq}), a synchronous-reference-frame phase-locked-loop (SRF-PLL), a DC link voltage feed-forward loop, and proportional + resonant (PR) inner voltage and current controllers (G_v and G_i). Inductive currents and capacitor voltages are transformed to the stationary reference frame ($i_{L\alpha\beta}$ and $v_{c\alpha\beta}$). Output currents are transformed to the SRF (i_{odq}). The direct and quadrature current outputs are independently controlled by the VR loop in dq axis. The inner voltage and current loops are implemented in $\alpha\beta$ frame. The power circuit consists of a three-leg three-phase inverter connected to a DC link, loaded by an L_f-C_f filter, and connected to the AC bus through a power line (Z_{line}).

The proposed controller provides a voltage reference to the inner loop. The voltage reference $\boldsymbol{V_{ref}}$ is generated by combining the amplitude reference ($|\boldsymbol{V_{ref}}|$) and the phase generated (θ) by the SRF-PLL.

In the case of supplying active loads, the direct current flowing through the VR will drop the direct voltage, causing a decrease in the output voltage amplitude. Hence, a droop characteristic is also imposed by the VR adapting the amplitude of output voltage, which endows to the system an I_{od}–V droop characteristic.

Even though the PLL is trying to synchronize the inverter with common AC bus, in the case of supplying reactive loads, the quadrature current flowing through the VR will produce an unavoidable quadrature voltage drop, which will cause an increase in PLL frequency. Thus, the mechanism inherently endows an I_{oq}-ω droop characteristic in each inverter.

The I_{oq}-ω and I_{od}–V droop characteristics in each inverter are used instead of adopting power droop controller. The relationship of I_{od}, I_{oq}, R_{vird}, and R_{virq} can be generalized and expressed for a number N of converters as follows [40]:

$$I_{od1}R_{vird1} = I_{od2}R_{vird2} = \cdots = I_{odN}R_{virdN} \quad (1a)$$

$$I_{oq1}R_{virq1} = I_{oq2}R_{virq2} = \cdots = I_{oqN}R_{virqN} \quad (1b)$$

The d- and q-axis current outputs I_{od} and I_{oq} of the paralleled inverters are inversely proportional to the corresponding VRs. Therefore, the direct and quadrature current outputs of each inverter can be regulated independently by adjusting the VRs based on different power rates, commands from energy management system (EMS) or other higher level control loops.

Furthermore, the active and reactive power outputs sharing strategy among the paralleled inverters can be obtained from (1) by multiplying the voltage reference. Considering that the voltage references (V_{ref}) of each inverter are equal, the active and reactive power outputs will also be properly shared based on the VRs, as shown in the following relationships:

$$P_{o1}R_{vird1} = P_{o2}R_{vird2} = \ldots = P_{oN}R_{virdN} \quad (2a)$$

$$Q_{o1}R_{virq1} = Q_{o2}R_{virq2} = \ldots = Q_{oN}R_{virqN} \quad (2b)$$

where P_{on} and Q_{on} are the active and reactive power outputs of inverter #n, n = 1, 2, …, N.

B. Proposed Balanced Discharge Rate Control Strategy

As discussed above in Section II, the conventional power-sharing control strategy for MG focuses on ensuring the equal power-sharing among different DG units. Therefore, the same VR (R_{vir}) is usually employed in all the DG units. However, the nominal capacities and SoC values of ESSs in DG units are usually different. The discharge rate of DG #i (η_i) can be defined as:

$$\eta_i = \frac{d}{dt}SoC_i = \frac{d}{dt}\left(1 - \frac{k}{C_{bati}}\int P_i dt\right) = -\frac{k}{C_{bati}}P_i \quad (3)$$

where k is the change ratio for a time scale and is equal to 1/3600, $C_{\text{bat}i}$ is the nominal capacity of the ESS$_i$, and P_i is the active power output of DG #i. Evidently, the discharge rate is influenced by the different nominal capacities of ESSs and the power output of DG #i. Thus, the discharge rate (η_i) can be adjusted to an equal value by regulating VRs (R_{viri}) based on their respective SoCs given that the load-sharing ratio

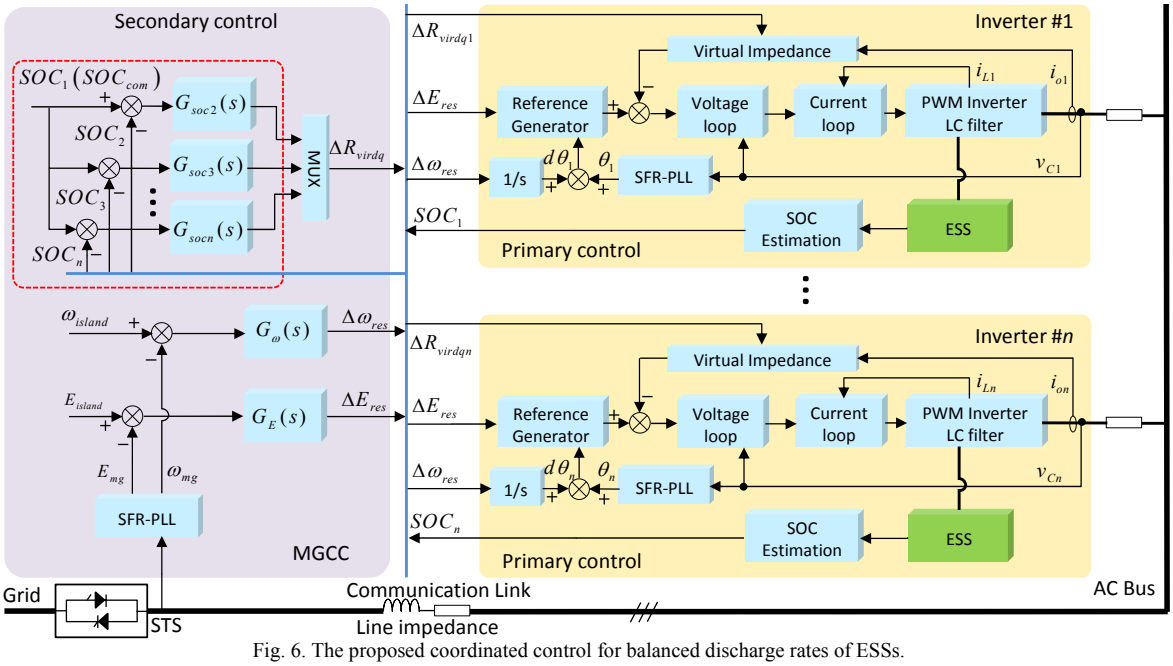

Fig. 6. The proposed coordinated control for balanced discharge rates of ESSs.

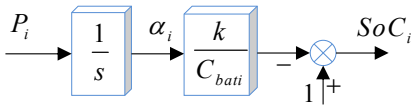

Fig. 7. Block diagram of the relationship between SoC and power output.

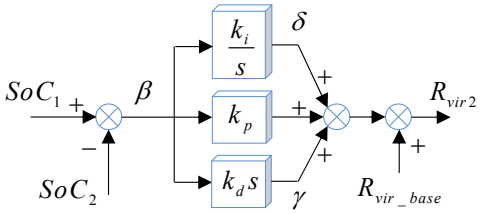

Fig. 8. Block diagram of the proposed coordinated secondary PID controller.

among DGs is dominated by the VR ratio. The control principle is illustrated in Fig. 5.

The detailed control scheme for the proposed coordinated SoC control strategy is shown in Fig. 6 [41], where $\Delta\omega_{res}$ and ΔE_{res} are used for restoring voltage and frequency deviations.

Hypothetically, ESSs are fully charged at the beginning, i.e., their initial SoC values are equal to 1. An additional coordinating control loop is added at the secondary control level in order to balance the discharge rate among DGs. The output of the SoC estimation loop is fed back to the secondary controller through the communication links. One of the DG units is selected as the common reference (SoC_{com}), whereas the remaining DG units adjust their VRs based on the differences between SoC_i and the common reference SoC_{com} with a PID controller expressed as follows:

$$\Delta R_{viri} = k_p(SoC_{com} - SoC_i) + k_i\int(SoC_{com} - SoC_i)dt + k_d\frac{d(SoC_{com} - SoC_i)}{dt} \quad (4)$$

where k_p, k_i, and k_d are the parameters of the PID controller.

The output of the PID controller is regarded as an incremental control component to reduce the power oscillation among DG units. Therefore, the adaptive VRs of each DG can be represented as follows:

$$R_{viri} = R_{vir\_base} + \Delta R_{viri} \qquad i = 2,3,4.....N \quad (5)$$

where R_{viri} is the VR of DG #i, R_{vir_base} is the preassigned VR, which is equal to 4 Ω according to [40], and ΔR_{viri} is the incremental output from the PID controller.

IV. Small-Signal Model and Stability Analysis

The state-space small-signal model of the proposed coordinated secondary controller for balancing discharge rate was developed to analyze system stability and parameter sensitivity.

The electrical energy consumption of ESS_i can be represented by the integration of the active power output of DG #i (P_i), as shown in Fig. 7. The state-space small-signal model can be derived as follows:

$$\Delta\hat{\alpha}_i = \Delta P_i \quad (6)$$

where $\hat{}$ denotes the derivative with respect to time.

The output equation for SoC_i can be written as:

$$SoC_i = 1 - \frac{k}{C_{bati}}\alpha_i \quad (7)$$

If two DG units are included in the MG and SoC_1 is considered as the common reference, the coordinated secondary controller for discharge rate balancing purposes can be illustrated by Fig. 8.

The small-signal models of variables β and δ are described in (8) according to Fig. 8.

$$\begin{cases} \hat{\Delta\beta} = \dfrac{1}{k_d}\Delta\gamma = \dfrac{k}{C_{bat2}}\Delta P_2 - \dfrac{k}{C_{bat1}}\Delta P_1 \\ \hat{\Delta\delta} = k_i\Delta\beta = \dfrac{k_i k}{C_{bat2}}\Delta\alpha_2 - \dfrac{k_i k}{C_{bat1}}\Delta\alpha_1 \end{cases} \tag{8}$$

Given that the basic values of the VRs of DG #1 and DG #2 are preset to 4 Ω, and the relationship between ΔP_1 and ΔP_2 can be represented as follows:

$$\Delta P_1 = (\Delta P_2 + \frac{P_2\Delta\delta}{4} + \frac{\delta\Delta P_2}{4} + \frac{2k_d k P_2}{4C_{bat2}}\Delta P_2 - \frac{k_d k P_1}{4C_{bat1}}\Delta P_2 + \frac{k_p P_2\Delta\beta}{4} + \frac{k_p\beta\Delta P_2}{4}) / (1 + \frac{k_d k}{4C_{bat1}}P_2) \tag{9}$$

The complete state-space model of MG can be derived by (10) by combining (6)-(9).

$$\Delta\hat{X} = A\Delta X + Bu \tag{10}$$

where $\Delta X = [\Delta\alpha_1 \quad \Delta\alpha_2 \quad \Delta\beta \quad \Delta\gamma]^T$,

$$A = \begin{bmatrix} 0 & 0 & \dfrac{k_p P_2 C_{bat1}}{4C_{bat1} + k_d k P_2} & \dfrac{P_2 C_{bat1}}{4C_{bat1} + k_d k P_2} \\ 0 & 0 & 0 & 0 \\ 0 & 0 & \dfrac{-k k_p P_2}{4C_{bat1} + k_d k P_2} & \dfrac{-k P_2}{4C_{bat1} + k_d k P_2} \\ \dfrac{-k_i k}{C_{bat1}} & \dfrac{k_i k}{C_{bat2}} & 0 & 0 \end{bmatrix}$$

Root locus plots of (10) are represented as a function of different parameter variations. Model parameters are listed in Table I.

Fig. 9 shows the root locus when k_p increases from 100 to 1500 while k_d changes from 1 to 100. The dynamic response and oscillation damping performance of the system are improved as k_p increases. When k_d increases, the complex poles move toward the real and imaginary axes, suppressing oscillation but at the same time slowing down the transient response.

Fig. 10 shows the trajectories of the modes when k_d increases from 1 to 300 while k_i also increases from 100 to 2000. The complex poles become the dominant modes, resulting in a nearly second-order behavior. The imaginary parts of the modes increase and move toward the imaginary axis as k_d and k_i increase, causing the system becoming more oscillatory.

Fig. 11 shows the trajectories of the modes in function of k_i, which increases from 100 to 2000, while k_p increases from 100 to 1500. When those parameter values increase, the dominant eigenvalues move away from the imaginary axis and thus the system dynamic response is improved.

As illustrated in Figs. 9 to 11, the paralleled DG units with the proposed control strategy remain stable within the parameter values region and present low sensitivity with the parameter variation at the secondary control level. The reason for this is the large stability margin provided by the autonomous current-sharing control at the primary level.

TABLE I
MODEL PARAMETERS

Symbol	value	Symbol	value	Symbol	value
k	1/3600	k_p	500	k_i	1000
k_d	10	C_{bat1}	100 Wh	C_{bat2}	200 Wh
$R_{vir\_base1/2}$	4 Ω	P_1	800 W	P_2	1600 W

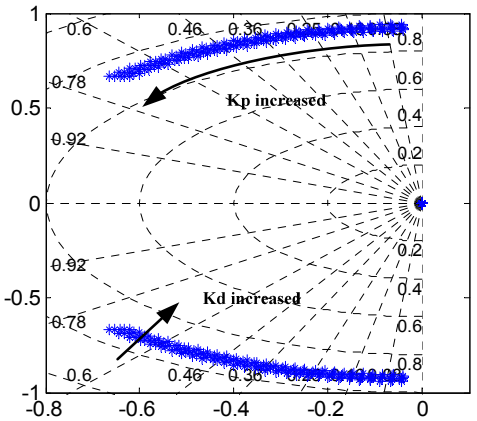

Fig. 9. Trace of nodes as a function of $1 \le k_d \le 100$ and $100 \le k_p \le 1500$.

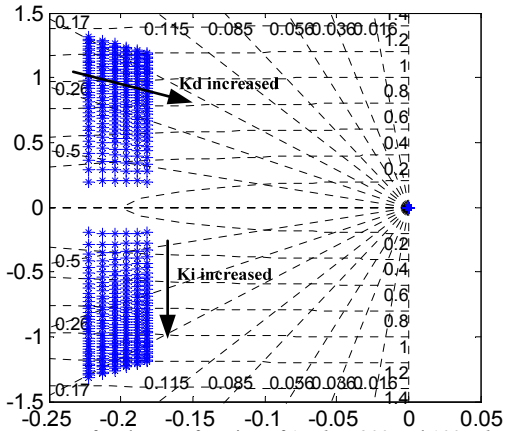

Fig. 10. Trace of nodes as a function of $1 \le k_d \le 300$ and $100 \le k_i \le 2000$.

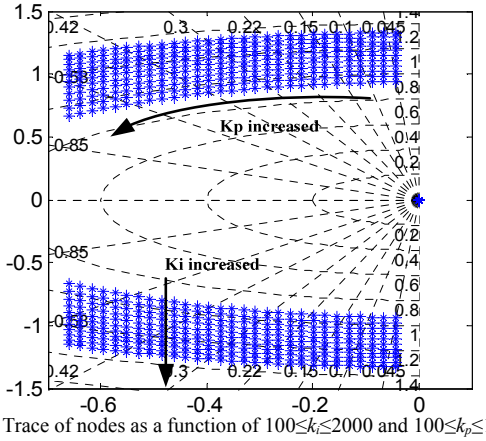

Fig. 11. Trace of nodes as a function of $100 \le k_i \le 2000$ and $100 \le k_p \le 1500$.

Therefore, the proposed control approach can achieve a more stable control performance than a coordinated secondary controller based on power droop control.

V. Simulation and Experimental Results

Simulations using MATLAB/Simulink and experiments based on a scaled-down islanded AC MG setup are conducted to compare and evaluate the performance of the proposed coordinated secondary control for balancing discharge rates. The simulation model is composed of three DGs with different ESSs and two local loads. The experimental platform consists of three Danfoss 2.2 kW inverters, a real-time control and monitoring platform, *LC* filters and two resistive loads, as shown in Fig. 12. The parameters for simulation and experiments are listed in Tables I and II.

The results are used to compare the control performance of the proposed control approach with that of the conventional power-sharing control.

Several required assumptions need to be met before the simulation and experiment are conducted according to the case-study scenario. Firstly, each ESS should be fully charged; thus, each initial SoC is equal to 1. Secondly, the minimum threshold of SoC is preset to 0.3, that is, DG #*i* will be shut down once its SoC becomes lower than 0.3 to avoid deep-discharge. This setting point can be adjusted according to the technology of the batteries and the recommended practices of the manufacturer.

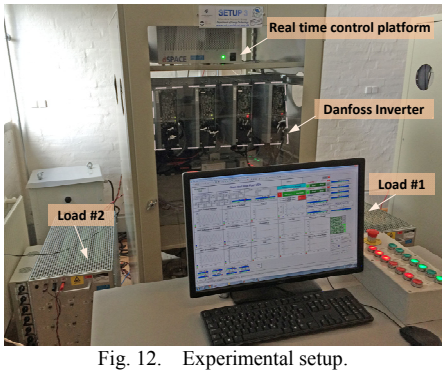

Fig. 12. Experimental setup.

TABLE II
Power Circuit and Control System Parameters

Parameters		Value
Symbol	**Description**	
DG Inverter, Output Filter, Loads and Line Impedance		
V_{dc}/ V_{MG}	DC voltage/ MG output voltage	650/ 311 V
f/ f_s	MG frequency / Switching frequency	50 / 10k Hz
L_f/ C_f	Filter inductance / capacitance	1.8 mH/ 25 μF
P_{max_E}	Maximum power output (experiment)	1 kW
P_{max_S}	Maximum power output (simulation)	4.5 kW
$R_{load\ E\ 1/2}$	Common load #1/2 (experiment)	230/230 Ω
$R_{load\ S\ 1/2}$	Common load #1/2 (simulation)	5000/3000 W
Primary control Loops		
k_{pi}	Proportional term in current controller	0.07
K_{ii}	Integral term in current controller	0
K_{pv}	Proportional term in voltage controller	0.04
K_{iv}	Integral term in voltage controller	94
$K_{p\ PLL}$	PLL proportional term	1.4
$K_{i\ PLL}$	PLL integral term	1000
Coordinated secondary control loop		
k_p/ k_i/ k_d	Proportional/ Integral/ Differential term	12/ 1000/ 10
$R_{vir\_base1/2/3}$	Basic values of VRs	4/4/4 Ω
$C_{bat\_E\_1/2/3}$	Battery capacities (experiment)	10/20/30 Wh
$C_{bat\_S\_1/2/3}$	Battery capacities (simulation)	100/200/300 Wh

A. Simulation Results with the Conventional Power-sharing Control

The simulation results with the conventional power-sharing control strategy are shown in Fig. 13. The active power output of each DG unit is controlled in order to share the loads equally. The SoC of each DG unit decreases at different rates, given that the nominal capacities of the ESSs ($C_{bat\_S\_1/2/3}$) are different. Note that, in this test, DG #1 has the smallest ESS capacity. Therefore, the SoC of DG #1 decreases faster. At 131 s, DG #1 is shut down when SoC_1 reaches 0.3 after a load step-up disturbance at 100 s, as shown in Fig. 13(a). The power outputs of DG #2 and DG #3

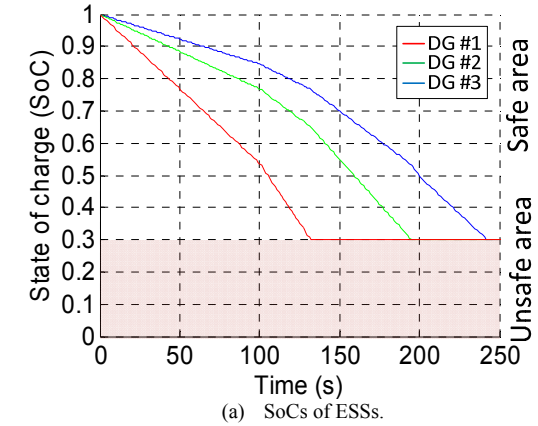

(a) SoCs of ESSs.

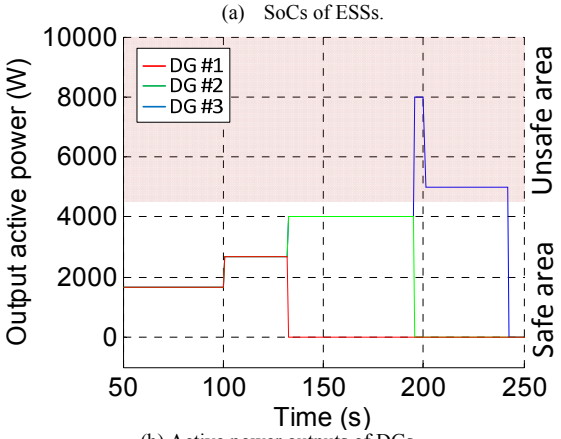

(b) Active power outputs of DGs.

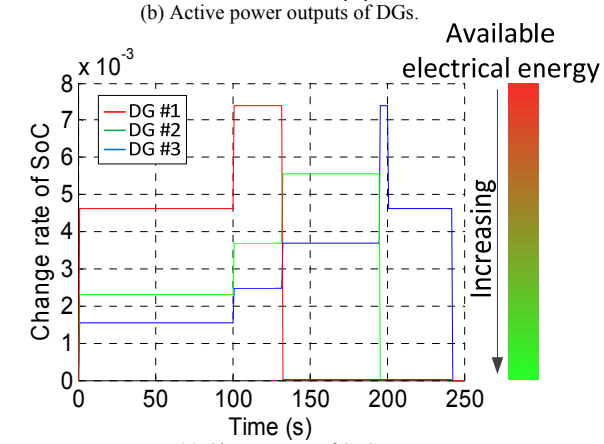

(c) Change rates of SoC.

Fig. 13. Simulation results with the conventional power-sharing control.

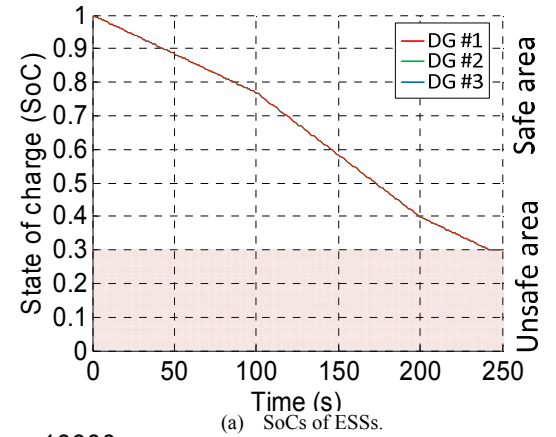

(a) SoCs of ESSs.

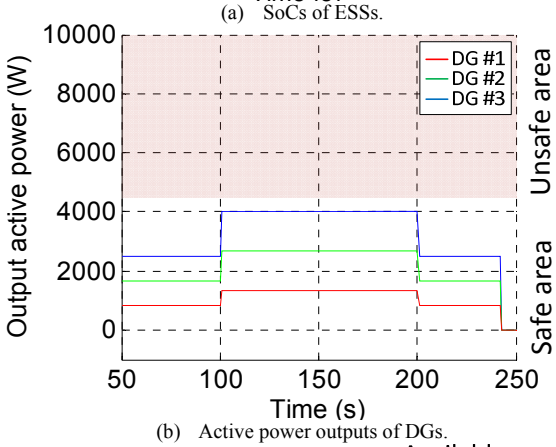

(b) Active power outputs of DGs.

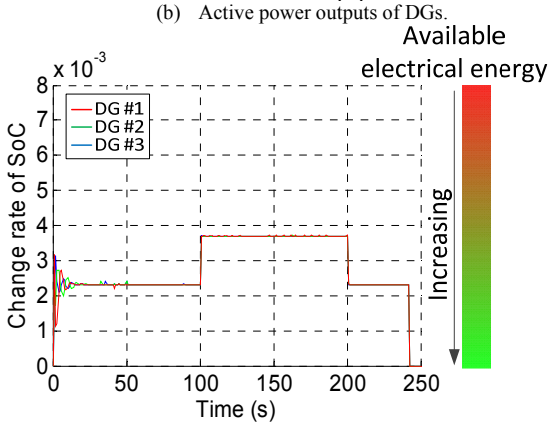

(c) Change rates of SoC

Fig. 14. Simulation results with the proposed coordinated controller.

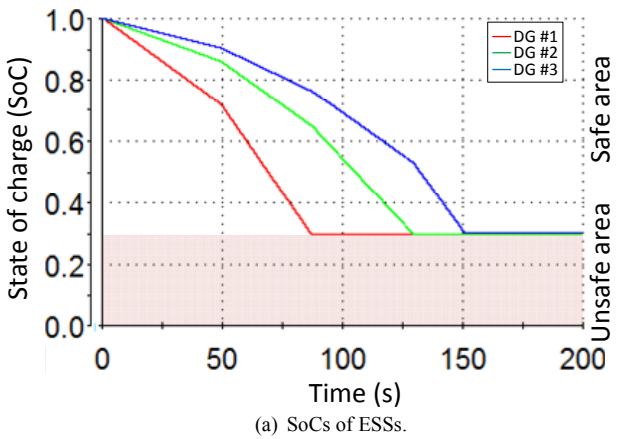

(a) SoCs of ESSs.

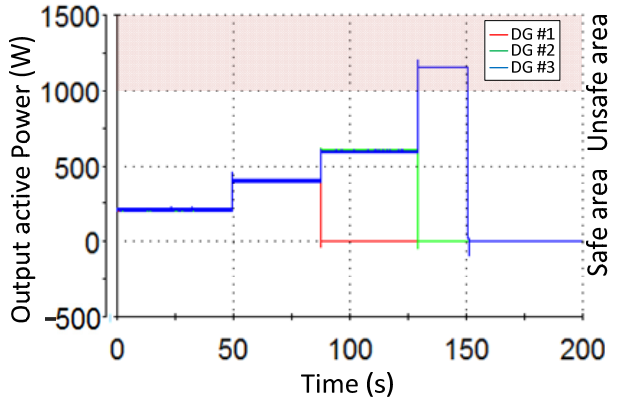

(b) Active power outputs of DGs.

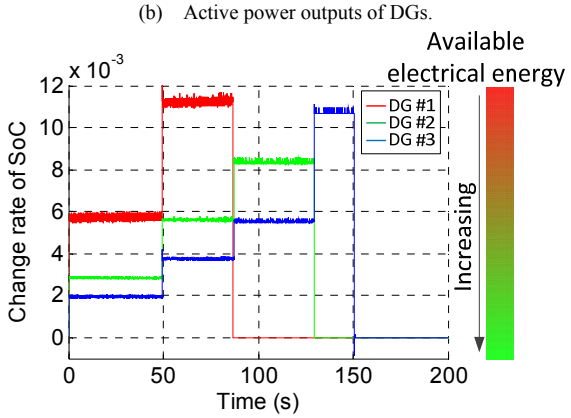

(c) Change rates of SoC.

Fig. 15. Experimental results with the conventional power-sharing control.

increase immediately to support the local loads, as shown in Figs. 13(b) and (c). At 193 s, DG #2 is shut down because SoC_2 is less than 0.3. The power output of DG #3 increases to 8 kW, which is significantly higher than the maximum power limitation (P_{max_S}), because DG #3 has to supply power to all the local loads after 193 s until it is disconnected from the common bus at 200 s. Obviously, a serious risk of operation failure because of overcurrent exists in real applications. Under this condition, the nominal capacities of all the DG units have to be increased for allowance to avoid affecting MG reliability. Moreover, in practice, the faster the ESSs discharge, the less the total electrical energy that can be obtained, as shown in Figs. 3 and 13(c).

B. Simulation Results with the Proposed Coordinated Secondary Controller

The simulation results with the proposed coordinated secondary control for balancing ESS discharge rate are shown in Fig.14. The VRs of DG #2 and DG #3 are regulated based on the outputs of the proposed coordinated secondary controller. In this way, SoC_1 to SoC_3 decrease in the same gradient and reach the protection threshold simultaneously, as shown in Figs. 14(a) and (c). It can be seen that the active power outputs of the DG units are different according to their respective SoCs, as shown in Fig. 14(b). Notably, no over current occurs, as illustrated in Fig. 14(b).

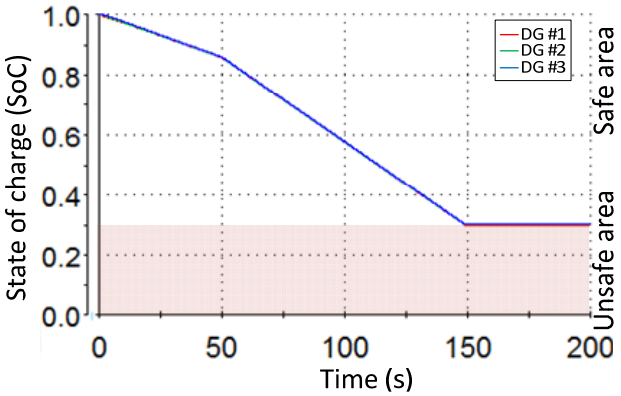

(a) SoCs of ESSs.

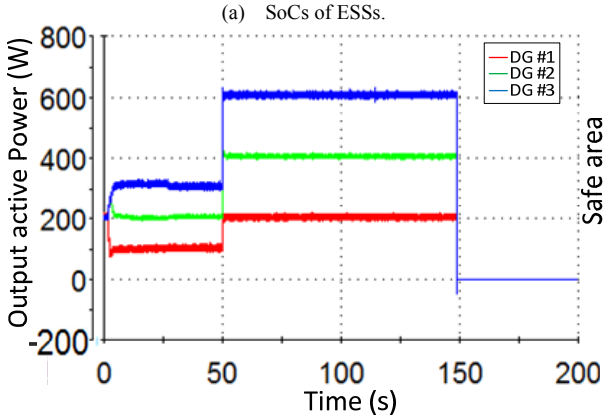

(b) Active power outputs of DGs.

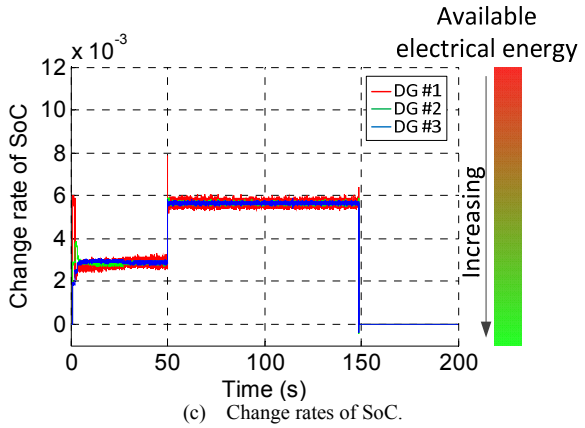

(c) Change rates of SoC.

Fig. 16. Experimental results with the proposed coordinated secondary controller.

C. *Experimental Results with the Conventional Power-sharing Control*

The experimental results with the conventional power-sharing control strategy are illustrated in Fig. 15. At the beginning, three paralleled DG units operate with equal power outputs by the conventional power-sharing control, which uses a unique VR in the primary control to supply common load #1. In this condition, their SoC values decrease at different rates because the nominal capacities of the ESSs are different. At 50 s, another extra 230 Ω load is connected to the parallel-connected DG system, causing a real power step change in each DG unit. With the unified power output, SoC_1 decreases the fastest because DG #1 has the lowest capacity. At 87 s, DG #1 is shut down as SoC_1 reaches 0.3, as shown in Fig. 15(a). Meanwhile, the real power outputs of DG #2 and DG #3 increase by 200 W, to supply the needed load, as shown in Fig. 15(b). At 129 s, DG #2 has also been shut down as SoC_2 reaches 0.3, leaving DG #3 to solely supply the total amount of needed power. As shown in Fig. 15(b), the power output of DG #3 has to increase to 1160 W, which is higher than the maximum power output (P_{max_E}) of each DG unit.

D. *Experimental Results with the Proposed Coordinated Secondary Controller*

Fig. 16 shows the experimental results of the SoC values, power outputs, and SoC change rates for the parallel-connected DG system with the proposed coordinated secondary controller. In this test, on the basis of the differences between the SoC of the common reference unit (DG #1) and the SoC values of the other DG units (DG #2 and DG #3), the VRs of DG #2 and DG #3 are regulated through the communication links. Therefore, the power outputs of the paralleled DG units are adjusted in terms of the different VRs. Fig. 16(a) shows that, at the beginning, three DG units are operating in a parallel mode without any coordinated control. After approximately 3 s, the proposed coordinated secondary controller initiates. Then, the SoC values decrease in the same gradient as the original point and simultaneously reach the protection threshold after the load step-up disturbance at 50 s. By contrast, the active power outputs of the DG units differ according to their SoCs, as shown in Fig. 16(b). Given that the ESS capacities of these three DG units are preset to 10, 20, and 30 Wh (at a ratio of 1:2:3), respectively, the load-power-sharing ratio among the parallel-connected DG units is also equal to 1:2:3. This control performance is guaranteed by the proposed coordinated secondary controller and the adaptive VRs in the primary control. Notably, overcurrent has never occurred during this test; thus, operation failure can be effectively prevented. Additionally, the redundant capacities and costs of the DG units can be reduced, and the reliability of the entire system can be improved. Furthermore, the lower discharge rates of the ESSs with the proposed coordinated secondary controller can help these ESSs provide higher available electrical energy, as shown in Fig. 16(c).

In summary, the theoretical analysis, root locus analysis, and the experimental results presented several improvements in comparison to the conventional power-sharing control and the earlier droop-based coordinated SoC control strategies. Firstly, the proposed SoC-balancing control strategy is developed in AC MGs instead of DC MGs. Secondly, it effectively guarantees SoC balancing to prevent overcurrent incidents and DGs unintentional outages in an AC MG. Thirdly, it provides a faster transient response and decoupled output-current-sharing because of the autonomous current-sharing control at the primary level. Fourth, it presents a lower sensitivity respect to secondary control level

TABLE III
PERFORMANCE COMPARISON

	Implementation	SoC rates balancing control capability	Transient response	Robustness	Communication cost
Power-sharing control	AC/ DC MG	No	Slow/ Fast	Good	No
Previous droop-based SoC rates balancing control	DC MG	Yes	Slow	Poor	Yes
Proposed SoC rates balancing control	AC MG	Yes	Fast	Good	Yes

parameters over the system dynamics due to the larger stability margin of the primary controller. The advantages and disadvantages of the proposed strategy compared with the conventional power-sharing control [8]-[13] and the previous droop-based coordinated SoC control [30]-[36] are summarized in Table III.

VI. CONCLUSIONS

This paper proposed a novel coordinated secondary control based on an autonomous current sharing control strategy for balancing the discharge rates of ESSs in islanded AC MGs. The coordinated secondary control can effectively prevent over-currents in DG units by regulating the power outputs of DG units according to their SoC values. In addition, the autonomous currents-sharing control strategy which is employed at the primary control level provided a faster transient response, more accurate output-current-sharing performance, and larger stability region than the earlier power droop control-based coordinated SoC control method. Simulation and experimental results obtained by using the conventional power-sharing control were compared with those obtained by using the proposed coordinated secondary control in order to verify the effectiveness of the proposed control approach.

REFERENCES

[1] Blaabjerg, F., Zhe Chen, Kjaer, S.B, "Power electronics as efficient interface in dispersed power generation systems," IEEE *Transactions on Power Electronics*, vol.2, no.2, pp. 1184-1194, 2004

[2] H. Farhangi, "The path of the smart grid," *IEEE Power Energy Mag*.,vol. 8, no. 1, pp. 18–28, Jan./Feb. 2010.

[3] "Technical paper—Definition of a set of requirements to generating units," *in UCTE*, 2008.

[4] Nikos Hatziargyriou, Hiroshi Asano, Reza Iravani, etc, "Microgrid," *IEEE power & energy magazine*, vol. 5, no.4, pp. 78-94, 2007

[5] R.H. Lasseter, "Microgrids", *in Proc. IEEE PES Winter Meeting* 2002, pp. 305-308.

[6] R. H. Lasseter and P. Paigi, "Microgrid: A conceptual solution," *in Proc. IEEE PESC*, Aachen, Germany, 2004, pp. 4285-4290.

[7] Piagi, P., Lasseter, R.H., "Autonomous control of microgrids," *Power Engineering Society General Meeting*, 2006. IEEE, vol., no., pp., 2006

[8] M. Chandorkar, D. Divan, and R. Adapa, "Control of parallel connected inverters in standalone ac supply systems," *IEEE Trans. Ind. Appl*., vol. 29, no. 1, pp. 136-143, Jan./Feb. 1993.

[9] A. Tuladhar, H. Jin, T. Unger, and K. Mauch, "Control of parallel inverters in distributed ac power systems with consideration of line impedance effect," *IEEE Trans. Ind. Appl*., vol. 36, no. 1, pp. 131-138, Jan./Feb. 2000.

[10] Yunwei Li, Vilathgamuwa, D.M., Poh Chiang Loh, "Design, Analysis, and Real-Time Testing of a Controller for Multibus Microgrid System," *IEEE Transactions on Power Electronics*, vol. 19, no. 5, pp. 1195–1204, Sept. 2004.

[11] R. Majumder, B. Chaudhuri, A. Ghosh, R. Majumder, G. Ledwich, and F. Zare, "Improvement of stability and load sharing in an autonomous microgrid using supplementary droop control loop," *IEEE Trans. Power Systems*, vol. 25, no. 2, pp. 796-808, May 2010.

[12] Vasquez, J.C., Guerrero, J.M., Luna, A., Rodriguez, P., "Adaptive Droop Control Applied to Voltage-Source Inverters Operating in Grid-Connected and Islanded Modes," *Industrial Electronics, IEEE Transactions on,* vol. 56, no. 10, 4088-4096, Oct. 2009.

[13] J. Guerrero, L. de Vicuna, J. Matas, M. Castilla, and J. Miret, "A wireless controller to enhsance dynamic performance of parallel inverters in distributed generation system," *IEEE Trans. Power Electron*., vol. 19, no. 5, pp. 1205–1213, Sep. 2004.

[14] R. H. Lasseter, A. Akhil, C. Marnay, J. Stephens, J. Dagle, R. Guttromson, A. Meliopoulous, R. Yinger, and J. Eto, "The CERTS Microgrid Concept," in *White paper for transmission reliability program*, Office of Power Technologies, U.S. Dept. Energy, Apr. 2002. Available: https://certs.lbl.gov/initiatives/certs-microgrid-concept

[15] K. Jong-Yul, J. Jin-Hong, K. Seul-Ki, C. Changhee, P. June-Ho, K. Hak- Man, and N. Kee-Young, "Cooperative control strategy of energy storage system and microsources for stabilizing the microgrid during islanded operation," *IEEE Trans. Power Electron*., vol. 25, no. 12, pp. 3037–3048, Dec. 2010.

[16] S. Adhikari and F. Li, "Coordinated V-f and P-Q control of solar photovoltaic generators with MPPT and battery storage in microgrids," *IEEE Trans. Smart Grid*, vol. 5, no. 3, pp. 1270–1281, May 2014.

[17] Y. Gurkaynak and A. Khaligh, "Control and power management of a grid connected residential photovoltaic system with plug-in hybrid electric vehicle (PHEV) load," *in Proc. IEEE Appl. Power Electron. Conf. Expo. (APEC)*, Washington, DC, USA, 2009, pp. 2086–2091.

[18] Ye Yang, Yang, N., Hui Li, "Cost-benefit study of dispersed battery storage to increase penetration of photovoltaic systems on distribution feeders," *PES General Meeting Conference & Exposition*, IEEE, National Harbor, MD, 2014

[19] B. S. Borowy and Z. M. Salameh, "Methodology for optimally sizing the combination of a battery bank and PV array in a wind/PV hybrid system," *IEEE Trans. Energy Convers*., vol. 11, no. 2, pp. 367–375, Jun. 1996.

[20] A. A. Al-Shamma'a and K. E. Addoweesh, "Optimum sizing of hybrid PV/wind/battery/diesel system considering wind turbine parameters using genetic algorithm," *in Proc. IEEE Int. Conf. Power Energy (IPECon)*, Kota Kinabalu, Malaysia, 2012, pp. 121–126.

[21] A. G. Cannone, D. O. Feder, and R. V. Biagetti, "Lead-Acid Batteries: Positive Grid Design Principles," *Bell System Technical Journal*, vol.49, no.7, pp.1279 – 1303, 1970.

[22] Kim J. Y., Jeon J. H., Kim S. K., Cho C. H., Park J. H., Kim H. M., and Nam K. Y., "Cooperative control strategy of energy storage system and microsources for stabilizing the microgrid during islanded operation," *IEEE Trans. Power Electron*., Vol. 25, No. 12, pp. 3037-3048, December 2010.

[23] Jong-Yul Kim; Seul-Ki Kim; Jin-Hong Jeon, "Coordinated state-ofcharge control strategy for microgrid during islanded operation," *Power Electronics for Distributed Generation Systems (PEDG), 2012 3rd IEEE International Symposium on*, pp.133-139, 25-28 June 2012

[24] Caldognetto, T., Tenti, P., Costabeber, A., Mattavelli, P, "Improving Microgrid Performance by Cooperative Control of Distributed Energy Sources," *IEEE Transactions on Industry Applications*, vol. 50, no. 6, pp. 3921 - 3930, Nov. 2014.

[25] H. Bode, *Lead Acid Batteries*. New York: Wiley, 1977.

[26] Guerrero, J.M., Chandorkar, M., Lee, T., Loh, P.C., "Advanced Control Architectures for Intelligent Microgrids—Part I: Decentralized and

Hierarchical Control," *Industrial Electronics, IEEE Transactions on*, vol.60, no.4, pp.1254-1262, April 2013.
[27] J. M. Guerrero, J. C. V´asquez, J. Matas, M. Castilla, de Vicuña, L.G., Castilla, M., "Hierarchical control of droop-controlled AC and DC microgrids—A general approach toward standardization," *IEEE Trans. Ind. Electron.*, vol. 58, no. 1, pp. 158–172, Jan. 2011.
[28] Y. A. R. I.Mohamed and A. A. Radwan, "Hierarchical control system for robust microgrid operation and seamless mode transfer in active distribution systems," *IEEE Trans. Smart Grid*, vol. 2, no. 2, pp. 352–362, Jun. 2011.
[29] Thale, S., Wandhare, R.G., Agarwal, V, "A Novel Reconfigurable Microgrid Architecture with Renewable Energy Sources and Storage," *IEEE Transactions on Industry Applications*, vol. 51, no. 2, pp: 1805-1816, March-April 2015.
[30] Xiaonan Lu, Kai Sun, Guerrero, J.M.; Vasquez, J.C.; Lipei Huang, "State-of-Charge Balance Using Adaptive Droop Control for Distributed Energy Storage Systems in DC Microgrid Applications," *Industrial Electronics, IEEE Transactions on*, vol.61, no.6, pp.2804,2815, June 2014
[31] T. Dragicevic, J. Guerrero, J. Vasquez, and D. Skrlec, "Supervisory control of an adaptive-droop regulated DC microgrid with battery management capability," *IEEE Trans. Power Electron.*, vol. 29, no. 2, pp. 695–706, Feb. 2013.
[32] Chendan Li, Dragicevic, T., Diaz, N.L., Vasquez, J.C., Guerrero, J.M., "Voltage scheduling droop control for State-of-Charge balance of distributed energy storage in DC microgrids," *Energy Conference (ENERGYCON), 2014 IEEE International*, 13-16 May 2014, Cavtat, pp: 1310-1314.
[33] Kakigano, H.; Miura, Y.; Ise, T., "Distribution Voltage Control for DC Microgrids Using Fuzzy Control and Gain-Scheduling Technique," *Power Electronics, IEEE Transactions on*, vol.28, no.5, pp.2246-2258, May 2013.
[34] Diaz, N.L., Dragicevic, T., Vasquez, J.C., Guerrero, J.M. "Intelligent Distributed Generation and Storage Units for DC Microgrids—A New Concept on Cooperative Control Without Communications Beyond Droop Control," *Smart Grid, IEEE Transactions on*, vol. 5, no. 5, pp: 2476 – 2485, Sept. 2014.
[35] N. L. Diaz, T. Dragicevic, J. C. Vasquez, J. M. Guerrero. "Fuzzy-logic-based gain-scheduling control for state-of-charge balance of distributed energy storage systems for DC microgrids," *Applied Power Electronics Conference and Exposition (APEC), 2014 Annual IEEE*, 16-20 Mar. 2014, Fort Worth, TX, pp: 2171 - 2176.
[36] Chendan Li, Garcia Plaza, M., Andrade, F., Vasquez, J.C., Guerrero, J.M., "Multiagent based distributed control for state-of-charge balance of distributed energy storage in DC microgrids," *Industrial Electronics Society, IECON* 2014, Oct. 29 2014-Nov. 1 2014, Dallas, pp: 2180 – 2184.
[37] Yasser Abdel-Rady Ibrahim Mohamed, Ehab F. El-Saadany. "Adaptive Decentralized Droop Controller to Preserve Power Sharing Stability of Paralleled Inverters in Distributed Generation Microgrids," *IEEE Transactions on Power Electronics*, vol. 23, no. 6, pp.2806-2816, Nov. 2008
[38] Yajuan Guan, Vasquez, J.C., Guerrero, J.M., Alves Coelho, E.A. "Small-signal modeling, analysis and testing of parallel three-phase-inverters with a novel autonomous current sharing controller," *Applied Power Electr. Conf. and Expo. (APEC)*, 2015 IEEE, pp. 571 – 578, Charlotte, NC, 15-19 Mar. 2015.
[39] N. Pogaku, M. Prodanovic, and T. C. Green, "Modeling, analysis and testing of autonomous operation of an inverter-based microgrid," *IEEE Trans. Power Electron.*, vol. 22, no. 2, pp. 613–625, Mar. 2007.
[40] Guan, Y., Guerrero, J.M., Zhao, X., Vasquez, J.C., Guo, X. "A New Way of Controlling Parallel-Connected Inverters by Using Synchronous-Reference-Frame Virtual Impedance Loop—Part I: Control Principle," *Power Electronics, IEEE Transactions on*, vol. 31, no. 6, pp: 4576 - 4593, June. 2016.
[41] Yajuan Guan, Josep M. Guerrero, Juan C. Vasquez. "Coordinated secondary control for balanced discharge rate of energy storage system in islanded microgrids," *Power Electronics and ECCE Asia (ICPE-ECCE Asia), 2015 9th International Conference on*, Seoul, Korea, June, 2015, pp. 475-481.

Yajuan Guan (S'14) received the B.S. degree and M.S. degree in Electrical Engineering from the Yanshan University, Qinhuangdao, Hebei, China, in 2007 and 2010 respectively. From 2010 to 2012, she was an Assistant Professor in Institute of Electrical Engineering (IEE), Chinese Academy of Sciences (CAS). Since 2013, she has been a Lecturer in IEE; CAS. She is currently working toward her Ph.D. degree at the Department of Energy Technology, Aalborg University, Denmark, as part of the Denmark Microgrids Research Programme (www.microgrids.et.aau.dk).
Her research interests include microgrids, distributed generation systems, power converter for renewable energy generation systems, and ancillary services for microgrids.

Juan C. Vasquez (M'12-SM'14) received the B.S. degree in electronics engineering from the Autonomous University of Manizales, Manizales, Colombia, and the Ph.D. degree in automatic control, robotics, and computer vision from the Technical University of Catalonia, Barcelona, Spain, in 2004 and 2009, respectively. He was with the Autonomous University of Manizales, where he taught courses on digital circuits, servo systems, and flexible manufacturing systems. He was also with the Technical University of Catalonia, as a Post-Doctoral Assistant, teaching courses based on renewable energy systems. In 2011, he was Assistant Professor in microgrids and currently he is working as an Associate Professor at the Department of Energy Technology, Aalborg University, Denmark. Dr. Vasquez is the co-responsible of the Research Program in Microgrids. From Feb. 2015 to April. 2015 he was a Visiting Scholar at the Center of Power Electronics Systems (CPES) at Virginia Tech.
His current research interests include operation, power management, hierarchical control, optimization and power quality applied to distributed generation and ac/dc microgrids. Dr. Vasquez is currently a member of the IEC System Evaluation Group SEG4 on LVDC Distribution and Safety for use in Developed and Developing Economies and the Renewable Energy Systems Technical Committee TC-RES in IEEE Industrial Electronics Society.

Josep M. Guerrero (S'01-M'04-SM'08-FM'15) received the B.S. degree in telecommunications engineering, the M.S. degree in electronics engineering, and the Ph.D. degree in power electronics from the Technical University of Catalonia, Barcelona, in 1997, 2000 and 2003, respectively. Since 2011, he has been a Full Professor with the Department of Energy Technology, Aalborg University, Denmark, where he is responsible for the Microgrid Research Program. From 2012 he is a guest Professor at the Chinese Academy of Science and the Nanjing University of Aeronautics and Astronautics; from 2014 he is chair Professor in Shandong University; and from 2015 he is a distinguished guest Professor in Hunan University.
His research interests is oriented to different microgrid aspects, including power electronics, distributed energy-storage systems, hierarchical and cooperative control, energy management systems, and optimization of microgrids and islanded minigrids. Prof. Guerrero is an Associate Editor for the IEEE TRANSACTIONS ON POWER ELECTRONICS, the IEEE TRANSACTIONS ON INDUSTRIAL ELECTRONICS, and the IEEE Industrial Electronics Magazine, and an Editor for the IEEE TRANSACTIONS on SMART GRID and IEEE TRANSACTIONS on ENERGY CONVERSION. He has been Guest Editor of the IEEE TRANSACTIONS ON POWER ELECTRONICS Special Issues: Power Electronics for Wind Energy Conversion and Power Electronics for

Microgrids; the IEEE TRANSACTIONS ON INDUSTRIAL ELECTRONICS Special Sections: Uninterruptible Power Supplies systems, Renewable Energy Systems, Distributed Generation and Microgrids, and Industrial Applications and Implementation Issues of the Kalman Filter; and the IEEE TRANSACTIONS on SMART GRID Special Issue on Smart DC Distribution Systems. He was the chair of the Renewable Energy Systems Technical Committee of the IEEE Industrial Electronics Society. In 2014 he was awarded by Thomson Reuters as Highly Cited Researcher, and in 2015 he was elevated as IEEE Fellow for his contributions on "distributed power systems and microgrids."